Nanocatalysis

International Edition: DOI: 10.1002/anie.201510355
German Edition: DOI: 10.1002/ange.201510355

Vacancy-Engineered Nanoceria: Enzyme Mimetic Hotspots for the Degradation of Nerve Agents

*Amit A. Vernekar, Tandrila Das, and Govindasamy Mugesh**

Abstract: *Organophosphorus-based nerve agents, such as paraoxon, parathion, and malathion, inhibit acetylcholinesterase, which results in paralysis, respiratory failure, and death. Bacteria are known to use the enzyme phosphotriesterase (PTE) to break down these compounds. In this work, we designed vacancy-engineered nanoceria (VE CeO_2 NPs) as PTE mimetic hotspots for the rapid degradation of nerve agents. We observed that the hydrolytic effect of the nanomaterial is due to the synergistic activity between both Ce^{3+} and Ce^{4+} ions located in the active site-like hotspots. Furthermore, the catalysis by nanoceria overcomes the product inhibition generally observed for PTE and small molecule-based PTE mimetics.*

Organophosphorous compounds are used extensively as pesticides, plasticizers, petroleum additives, and chemical warfare agents.[1] In particular, organophosphate triesters, such as paraoxon, parathion, and malathion, are employed in agriculture as crop protectants, but they are potentially toxic and can cause nerve shock, paralysis, respiratory failure, and death.[2] These nerve agents inhibit the key enzyme acetylcholinesterase involved in neuronal signaling (Scheme 1).[3]

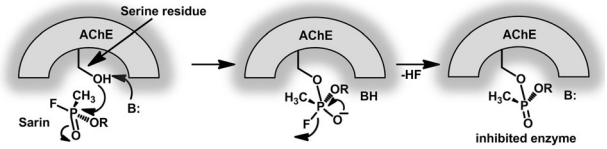

Scheme 1. Inhibition of acetylcholinesterase (AChE) by sarin (B = base).

They are also known to cause severe oxidative stress in humans and are associated with neurological disorders. Therefore, decontamination of these nerve agents is a world-wide concern, and many research teams have focused their attention to address this important problem.[4] Interestingly, bacteria use enzymes such as phosphotriesterases (PTE) to degrade organophosphorous esters and survive in soil under environmentally toxic conditions.[5]

[*] Dr. A. A. Vernekar, T. Das, Prof. Dr. G. Mugesh
Department of Inorganic and Physical Chemistry
Indian Institute of Science
Bangalore-560012 (India)
E-mail: mugesh@ipc.iisc.ernet.in

Supporting information and ORCID(s) from the author(s) for this article are available on the WWW under http://dx.doi.org/10.1002/anie.201510355.

Metal complexes, heterogeneous catalysts, metal organic frameworks, and a few nanomaterials have been shown to hydrolyze organophosphorus triesters.[4,6] However, in most of these cases, the activity is irreversibly inhibited by the reaction products, particularly phosphodiesters, thereby limiting their catalytic efficiency. Therefore, development of engineered nanomaterials for efficient degradation of nerve agents is important. As current interest in the field of nanobiomimetics is focused on the development of nanozymes,[7] we focused our attention to the generation of catalytic hotspots on the surface of nanoparticles. Herein, we report that the vacancy-engineered nanoceria (VE CeO_2 NPs) with cerium ions in dual oxidation states in the hotspots efficiently catalyze the hydrolysis of nerve agents and thus provide a potential degradation pathway.

VE CeO_2 NPs were prepared by following a method reported earlier with modification.[8] Addition of H_2O_2 during the synthesis resulted in VE CeO_2 NPs. The as-prepared VE CeO_2 NPs were then characterized by several methods. The X-ray diffraction (XRD) pattern (Figure 1 a) shows the peaks that can be indexed to CeO_2 (JCPDS 34-0394). Energy dispersive X-ray (EDX) spectra (Supporting Information, Figure S1) shows the peaks owing to Ce ions. Transmission electron microscopy (TEM; Figure 1 b) and high-resolution TEM images (Figure 1 c) revealed the particle size to be approximately 6 nm, with d spacing of 0.31 nm corresponding to 111 plane of CeO_2. The magnified high-resolution TEM image (Figure 1 d; Supporting Information, Figure S2) clearly shows the presence of defects/vacancies as hotspots formed on the surface of nanoceria. Compact and smaller particles are generally regarded to possess large surface energy in nanoform. Therefore, the system tends to attain low energy by eliminating some ions and creating defects in the material. A pictorial representation of the atomic arrangement of ions in VE CeO_2 NPs is shown in Figure 1 e.[9] The selected area electron diffraction (SAED) pattern shows distinct rings, confirming the polycrystallinity of the material (Figure 1 d inset). These rings can be indexed to CeO_2 and are in agreement with the XRD pattern. The defects in VE CeO_2 NPs were further probed using FT-Raman spectroscopy. The appearance of a broad peak around 600 cm^{-1} is attributed to defects on the surface of VE CeO_2 NPs (Figure 1 f). As the removal of oxygen atoms from the surface of a material results in the reduction of adjacent metal ions,[9] we recorded X-ray photoelectron spectra (XPS) of VE CeO_2 NPs. The Ce3d XPS spectra (Figure 1 g) reveal the presence of Ce ions in different oxidation states. The amount of Ce^{3+} present on the surface was estimated to be around 14.28 %.

VE CeO_2 NPs have been shown to catalyze CO oxidation[9] and to act as a superoxide dismutase (SOD) mime-

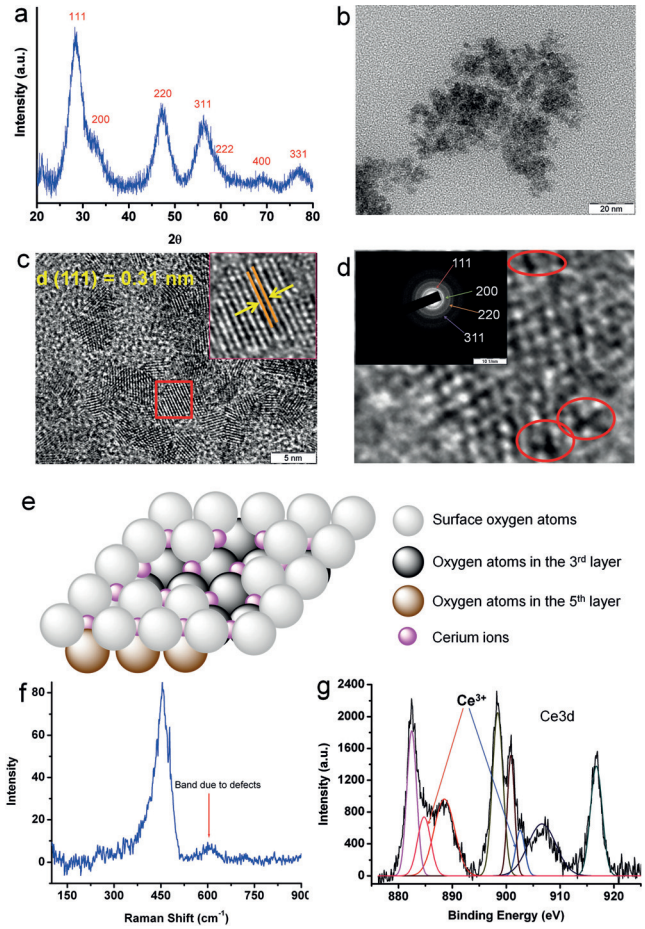

Figure 1. a) XRD pattern, b) TEM image (scale bar = 20 nm), c) HRTEM image (scale bar = 5 nm), and d) Magnified high resolution TEM image of VE CeO_2 NPs, inset shows SAED pattern (scale bar = 10 nm^{-1}). e) Representation of hotspots/vacancies on the surface of VE CeO_2 NPs; f) Raman spectra and g) Ce3d XPS of VE CeO_2 NPs.

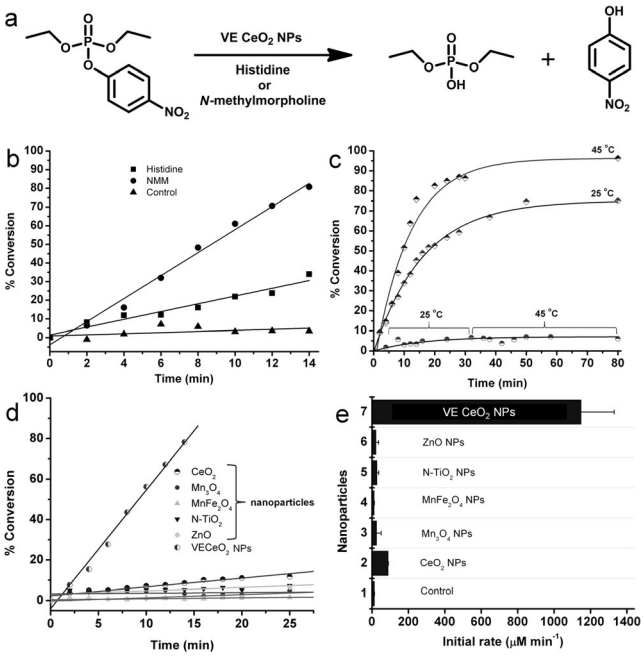

Figure 2. a) Reaction showing hydrolysis of paraoxon by VE CeO_2 NPs in the presence of histidine or *N*-methylmorpholine (NMM) base. b) Comparison of PTE-like activity of VE CeO_2 NPs in the presence of histidine and NMM as distal/proximal bases. c) PTE-like activity in the absence (circles) and presence (squares) of VE CeO_2 NPs at different temperatures. d) Comparison of PTE-like activity of various nanomaterials. e) initial rates corresponding to the plot shown in d.

tic.[7f,8,10] However, the use of VE CeO_2 NPs in solution phase for mimicking hydrolytic enzymes has not been investigated in detail. The PTE activity of VE CeO_2 NPs was measured by following the formation of *p*-nitrophenolate using UV/Vis spectroscopy at 401 nm. When the aqueous solution of phosphotriester, paraoxon, was treated with VE CeO_2 NPs, no hydrolysis was observed at 25 °C and 45 °C (Figure 2 a–c). However, when histidine was added to the reaction medium, VE CeO_2 NPs exhibited PTE-like activity (Figure 2 b), confirming that the histidine plays a crucial role in the catalysis by acting as a general base, similar to its role as a general base in enzyme catalysis.[11] However, the PTE-like activity in the presence of histidine was found to be low, probably owing to the poor solubility of histidine in the reaction medium. The precipitate thus formed can block the surface active site of VE CeO_2 NPs. Therefore, we employed *N*-methylmorpholine (NMM) as a general base for the reaction. Addition of NMM enhanced the hydrolytic activity at 25 °C and 45 °C significantly, which is probably due to the activation of metal-bound water molecules by polarization (Figure 2 c). When the concentration of NMM was increased from 0.1 M to 0.45 M, no significant change in the pH of the solution (around pH 10) or reaction rate was observed (Table S1). As no significant reaction was observed in NaOH solution or sodium carbonate–bicarbonate buffer at pH 10 without NMM, it can be assumed that NMM acts as a general base in the reaction. This was further confirmed by using imidazole and triethylamine, both of which enhanced the rate of reaction (Table S1). Although it is important to carry out the experiments at relatively higher pH, the nitrogen-containing bases play an important role in the catalytic process, that is, deprotonation of the activated water molecule. The hydrolysis of paraoxon was also studied by ^{31}P NMR spectroscopy in a time-dependent manner. As shown in Figure S3, the signal at −7.8 ppm for paraoxon decreased with time upon addition of VE CeO_2 NPs with a new peak appearing at −0.3 ppm for the diethylphosphate. In this reaction, no further hydrolysis was observed, indicating that the VE CeO_2 NPs are very selective phosphotriesterase model systems. The VE CeO_2 NPs also catalyze the hydrolysis (studied by ^{31}P NMR) of other phosphotriesters, such as methyl paraoxon and *p*-nitrophenyl diphenyl phosphate (Figure S10 and S11).

Vacancies in the material generally result in dual oxidation states of metal ions that are exposed to the reaction environment. As VE CeO_2 NPs have surfaces with exposed Ce^{3+} and Ce^{4+} ions, we studied the hydrolysis of paraoxon by other nanoparticles containing metal ions in two oxidation states, such as Mn_3O_4 and $MnFe_2O_4$ nanoparticles. We also studied other metal oxide nanoparticles, such as ZnO and *N*-TiO_2. However, these nanomaterials were found to be

inefficient in catalyzing the hydrolysis of paraoxon (Figure 2d,e). The bare CeO_2 nanoparticles prepared by precipitation without the use of H_2O_2 showed very poor activity (Figure 2d,e). These observations suggest that the type of metal ions with dual oxidation states and the catalytic hotspots are very important for capturing the substrate and activating them at the active sites. An optimum level of mixed valency of Ce at the catalytic sites is required for an efficient degradation process. The presence of metal ions in two different oxidation states may also help in the elimination of reaction products from the reaction sites.

The uncatalyzed reaction was extremely slow at 25 °C, and it remained slow even at higher temperatures (45 °C) (Figure 2c). However, the activity in the presence of VE CeO_2 NPs was found to be remarkably high and temperature-dependent (Figure 3a; Supporting Information, Figure S4).

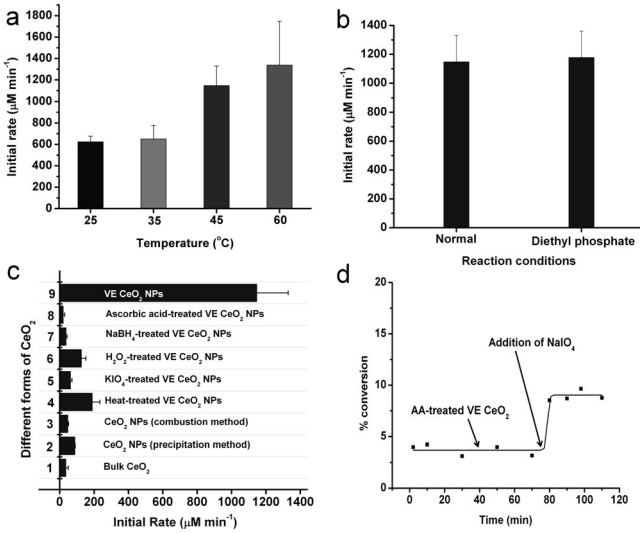

Figure 3. a) Comparison of initial rates of degradation of paraoxon by VE CeO_2 NPs at different temperatures. b) Effect of externally added diethyl phosphate on the initial rate. c) Comparison of initial rates of degradation of paraoxon by different forms of CeO_2 NPs. d) Addition of $NaIO_4$ to the reaction mixture containing ascorbic acid (AA)-treated VE CeO_2 NPs.

The $t_{1/2}$ values (time required to hydrolyze 50% of the paraoxon) for the reaction were found to be 17.8 min and 9.4 min at 25 °C and 45 °C, respectively. Furthermore, a large fluctuation in the initial rates was observed at 60 °C (Figure 3a), which is probably due to the differential surface adsorption of paraoxon at this temperature. Therefore, 45 °C was considered to be the optimum temperature for the degradation reactions. The activation energy for the hydrolysis was calculated to be 20.2 kJ mol^{-1} (Figure S5a). The sigmoidal nature of the plots shown in Figure S5b,c indicates that the VE CeO_2 NPs act as multivalent or cooperative catalysts.[12] At certain concentrations, the interactions between the nanoparticles appear to play an important role in enhancing the rate of the reaction. Such catalyst-dependent sigmoidal behavior has been ascribed to the formation of enzyme dimer or oligomers.[12b] We further studied the steady-state kinetics of the hydrolysis while keeping the concentration of the VE CeO_2 NPs constant (4.8 μM). In this case, a typical Michaelis–Menten plot was obtained when the concentration of paraoxon solution was increased from 5 to 50 mM (Figure S5d). Furthermore, the straight line in the Lineweaver–Burk plot (Figure S5e) suggests that the VE CeO_2 NPs follow enzyme-like kinetics. The kinetic parameters obtained from these plots show significantly high maximum velocity ($V_{max} = 1.56$ mM min^{-1}) and K_M (15.78 mM) values. Although a high value of K_M indicates low affinity of VE CeO_2 NPs towards paraoxon, this observation suggests that the weak binding of organophosphates may help in a facile elimination of the product from the reaction sites. By using the standard molar concentrations of nanoparticles, the turnover number (k_{cat}) and catalytic efficiency (k_{cat}/K_M) were found to be 5.42 s^{-1} and 3.44×10^2 M^{-1}s^{-1}, respectively.[13] These values are significantly higher than those reported for some metal complexes,[6c] and are comparable to native PTE enzyme.[14] The poor catalytic activity of many PTE mimetics is due to the inhibition of hydrolysis by the phosphodiesters produced in the reactions. Product inhibition is, therefore, a challenging problem in the development of catalysts for the degradation of nerve agents.[6b,c,15] Interestingly, when we tested the hydrolytic activity of VE CeO_2 NPs in the presence of high concentration of externally added diethyl phosphate (5 mM), the initial rate was not affected (Figure 3b), indicating that the catalytic sites are not blocked by the product. The inability of diethyl phosphate to interact with the active sites may also be responsible for its stability against further hydrolysis.

Interestingly, the activities of bulk CeO_2 or the CeO_2 NPs prepared by precipitation and combustion methods were found to be significantly lower than that obtained for VE CeO_2 NPs (Figure 3c). Although the sizes of the NPs are quite similar, the higher activity of VE CeO_2 NPs may be attributed to the presence of vacancies that act as catalytic hotspots. As the removal of surface oxygen atoms is balanced by the reduction of Ce^{4+} to Ce^{3+}, the activity of chemically-treated forms of VE CeO_2 NPs was tested. In one case, we treated the material with H_2O_2 or KIO_4 to oxidize most of the Ce^{3+} to Ce^{4+},[14] and in other case, the material was treated with ascorbic acid and $NaBH_4$ to reduce Ce^{4+} to Ce^{3+}.[16] In both the cases, the activity was found to be significantly lower than that of VE CeO_2 NPs having the metal in mixed oxidation states (Figure 3c). Furthermore, a sharp increase in the product formation was observed when sodium periodate ($NaIO_4$, 5 mM final concentration) was added to the reaction mixture containing ascorbic acid-treated VE CeO_2 NPs (Figure 3d). This observation indicates that the oxidation of some of the Ce^{3+} ions to Ce^{4+} is responsible for the enhancement in the hydrolysis. After the initial increase in the hydrolysis, the reaction becomes relatively slower when most of the Ce^{3+} ions are oxidized to Ce^{4+} by $NaIO_4$.

The unique chemistry observed for VE CeO_2 NPs is due to the selective and preferential binding of water and paraoxon with Ce ions in different oxidation states. The material having only Ce^{4+} ions would allow the binding of paraoxon in all vacant sites owing to the polar nature of phosphoryl oxygen

(Figure S6), but the binding and activation of water molecules is disfavored in such material. On the other hand, materials with a large number of Ce^{3+} ions would allow selective adsorption of H_2O molecules and prevent the adsorption of paraoxon (Figure S6). When cerium ions are present in mixed oxidation states, the preferential binding of H_2O at Ce^{3+} sites and paraoxon at Ce^{4+} sites allows an efficient nucleophilic attack of water (or hydroxide) at the phosphorus center (Figure 4a). The catalytic cycle can continue multiple times as the VE CeO_2 NPs are highly stable. The identical XRD patterns of the as-prepared VE CeO_2 NPs and recovered NPs (Figure 4b) indicate that the material characteristics are not lost during the catalysis. The TEM, HRTEM, and SAED pattern of the recovered NPs (Figure 4c; Supporting Information, Figure S9) also reveal that the catalytic hotspots are intact.

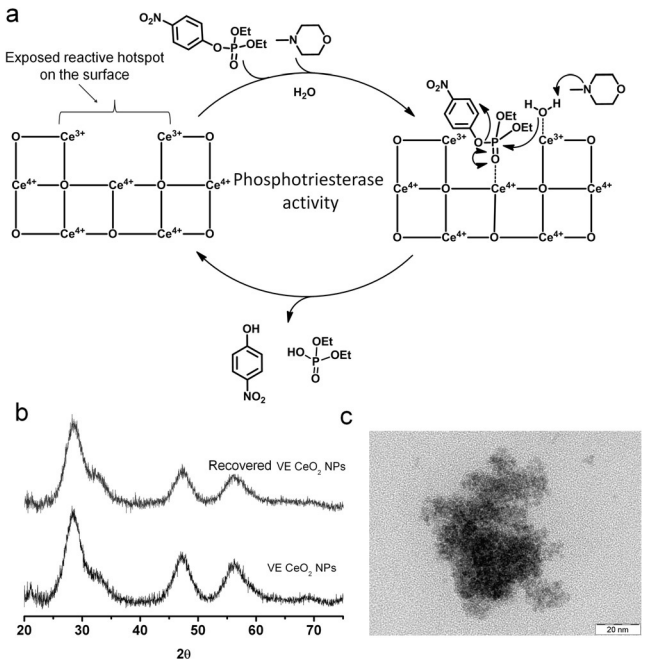

Figure 4. a) Proposed mechanism for the degradation of phosphotriesters by VE CeO_2 NPs. b) comparison of the XRD patterns of VE CeO_2 NPs and recovered catalyst. c) TEM image of the recovered VE CeO_2 NPs showing the nanoparticles are intact.

To exclude the possibility of leached Ce ions exhibiting PTE-like activity, we measured the rate of hydrolysis using solutions of Ce^{3+} and Ce^{4+} salts separately. Although the concentration of Ce ions was kept sufficiently higher than that in VE CeO_2 NPs, the activity was found to be very low (Figure S7a). When the concentration of Ce^{3+} ions was increased almost 600 times more than that of VE CeO_2 NPs, a small increase in the activity was observed. On the other hand, no significant activity was observed when the reaction was carried out with only Ce^{4+} ions (Figure S7b) or with a mixture of Ce^{3+} and Ce^{4+} ions (Figure S7c). Similarly, addition of Ce^{3+} ions to the reaction mixture containing CeO_2 NPs having fewer defects and more Ce^{4+} ions does not increase the catalytic activity (Figure S8). These observations suggest that the hydrolysis occurs at the surface of the nanomaterial, and that a well-defined active site is required for the catalysis. For this reason, the heat-treated VE CeO_2 NPs also exhibited significantly lower activity (Figure 3c). It is expected that heating the material at high temperature results in lattice ordering and minimization of defects, leading to blockage of catalytic sites.

In conclusion, we have shown that enzyme mimetic hotspots can be generated in nanoceria by removing a few oxygen atoms. The vacancy-engineered ceria nanoparticles developed by this method catalyze the degradation of potentially harmful nerve agents, such as paraoxon with high efficiency. This study constitutes the first example of a hydrolysis reaction by a vacancy-engineered nanomaterial in which the dual oxidation states of metal ions play a crucial role. A detailed mechanistic investigation revealed that the presence of both Ce^{3+} and Ce^{4+} ions on the surface, and the distance between these two ions, play an important role in the catalysis.

Acknowledgements

This study was supported by the Science and Engineering Research Board (SERB), New Delhi.

Keywords: enzyme models · heterogeneous catalysis · nanozymes · nerve agents · phosphotriesterase

How to cite: *Angew. Chem. Int. Ed.* **2016**, *55*, 1412–1416
Angew. Chem. **2016**, *128*, 1434–1438

[1] a) R. M. Black, J. M. Harrison in *The Chemistry of Organophosphorus Compounds*, *Vol. 4* (Ed.: F. R. Hartley), Wiley, Chichester, **1996**, pp. 781–840; b) J. Svara, N. Weferling, T. Hofmann, *Phosphorus Compounds*, *Organic*, *Ullmann's Encyclopedia of Industrial Chemistry*, Wiley-VCH, Weinheim, **2006**; c) S. M. Somani, R. P. Solana, S. N. Dube in *Chemical Warfare Agents* (Ed.: S. M. Somani), Academic Press, San Diego, **1992**, pp. 68–123.

[2] a) M. B. Abou-Donia, *Arch. Environ. Health* **2003**, *58*, 484–497; b) M. Eddleston, N. A. Buckley, P. Eyer, A. H. Dawson, *Lancet* **2008**, *371*, 597–607; c) J. E. Compston, S. Vedi, A. B. Stephen, S. Bord, A. R. Lyons, S. J. Hodges, B. E. Scammell, *Lancet* **1999**, *354*, 1791–1792; d) M. C. Alavanja, J. A. Hoppin, F. Kamel, *Annu. Rev. Public Health* **2004**, *25*, 155–197.

[3] D. M. Maxwell, K. M. Brecht, I. Koplovitz, R. E. Sweeney, *Arch. Toxicol.* **2006**, *80*, 756–760.

[4] a) Y. C. Yang, J. A. Baker, J. R. Ward, *Chem. Rev.* **1992**, *92*, 1729–1743; b) K. Kim, O. G. Tsay, D. A. Atwood, D. G. Churchill, *Chem. Rev.* **2011**, *111*, 5345–5403; c) M. J. Katz, J. E. Mondloch, R. K. Totten, J. K. Park, S. T. Nguyen, O. K. Farha, J. T. Hupp, *Angew. Chem. Int. Ed.* **2014**, *53*, 497–501; *Angew. Chem.* **2014**, *126*, 507–511; d) J. E. Mondloch, M. J. Katz, W. C. Isley III, P. Ghosh, P. Liao, W. Bury, G. W. Wagner, M. G. Hall, J. B. DeCoste, G. W. Peterson, R. Q. Snurr, C. J. Cramer, J. T. Hupp, O. K. Farha, *Nat. Mater.* **2015**, *14*, 512–516; e) S.-Y. Moon, Y. Liu, J. T. Hupp, O. K. Farha, *Angew. Chem. Int. Ed.* **2015**, *54*, 6795–6799; *Angew. Chem.* **2015**, *127*, 6899–6903.

[5] B. K. Singh, *Nat. Rev. Microbiol.* **2009**, *7*, 156–164, and references therein.

[6] a) N. V. Kaminskaia, C. He, S. J. Lippard, *Inorg. Chem.* **2000**, *39*, 3365–3373; b) A. Tamilselvi, G. Mugesh, *Chem. Eur. J.* **2010**, *16*,

8878 – 8886; c) C. M. Hartshorn, A. Singh, E. L. Chang, *J. Mater. Chem.* **2002**, *12*, 602 – 605; d) T. S. Keizer, L. J. De Pue, S. Parkin, D. A. Atwood, *J. Am. Chem. Soc.* **2002**, *124*, 1864 – 1865; e) G. W. Wagner, P. W. Bartram, O. Koper, K. J. Klabunde, *J. Phys. Chem. B* **1999**, *103*, 3225 – 3228; f) A. Michalkova, Y. Paukku, D. Majumdar, J. Leszczynski, *Chem. Phys. Lett.* **2007**, *438*, 72 – 77; g) B. B. Dhar, D. R. Edwards, R. S. Brown, *Inorg. Chem.* **2011**, *50*, 3071 – 3077.

[7] a) F. Manea, F. B. Houillon, L. Pasquato, P. Scrimin, *Angew. Chem. Int. Ed.* **2004**, *43*, 6165 – 6169; *Angew. Chem.* **2004**, *116*, 6291 – 6295; b) L. Gao, J. Zhuang, L. Nie, J. Zhang, Y. Zhang, N. Gu, T. Wang, J. Feng, D. Yang, S. Perrett, X. Yan, *Nat. Nanotechnol.* **2007**, *2*, 577 – 583; c) F. Natalio, R. André, A. F. Hartog, B. Stoll, K. P. Jochum, R. Wever, W. Tremel, *Nat. Nanotechnol.* **2012**, *7*, 530 – 535; d) K. Fan, C. Cao, Y. Pan, D. Lu, D. Yang, J. Feng, L. Song, M. Liang, X. Yan, *Nat. Nanotechnol.* **2012**, *7*, 459 – 464; e) A. A. Vernekar, G. Mugesh, *Chem. Eur. J.* **2012**, *18*, 15122 – 15132; f) H. Wei, E. Wang, *Chem. Soc. Rev.* **2013**, *42*, 6060 – 6093, and references therein; g) A. A. Vernekar, G. Mugesh, *Chem. Eur. J.* **2013**, *19*, 16699 – 16706; h) A. A. Vernekar, D. Sinha, S. Srivastava, P. U. Paramasivam, P. D′Silva, G. Mugesh, *Nat. Commun.* **2014**, *5*, 5301.

[8] C. Korsvik, S. Patil, S. Seal, W. T. Self, *Chem. Commun.* **2007**, 1056 – 1058.

[9] a) N. Lawrence, J. Brewer, L. Wang, T. Wu, J. Wells-Kingsbury, M. Ihrig, G. Wang, Y. Soo, W. Mei, C. Cheung, *Nano Lett.* **2011**, *11*, 2666 – 2671; b) Y. Sun, Q. Liu, S. Gao, H. Cheng, F. Lei, Z. Sun, Y. Jiang, H. Su, S. Wei, Y. Xie, *Nat. Commun.* **2014**, *5*, 2899.

[10] a) E. Heckert, A. Karakoti, S. Seal, W. T. Self, *Biomaterials* **2008**, *29*, 2705 – 2709; b) C. Xu, X. Qu, *NPG Asia Mater.* **2014**, *6*, *e90.*

[11] a) E. J. Crane, D. Prasonage, A. Claiborne, *Biochemistry* **1996**, *35*, 2380 – 2387; b) G. Dodson, A. Wlodawer, *Trends Biochem. Sci.* **1998**, *23*, 347 – 352.

[12] a) C. Guarise, F. Manea, G. Zaupa, L. Pasquato, L. J. Prins, P. Scrimin, *J. Pept. Sci.* **2008**, *14*, 174 – 183; b) L. F. Cavalieri, M. J. Modak, S. K. Marcus, *Proc. Natl. Acad. Sci. USA* **1974**, *71*, 858 – 862.

[13] From the Raman spectrum (Figure 1 f), it is found that the number of oxygen vacancies per nanoparticle is around 388, which may correspond to the number of active sites. V. Prabhakaran, V. Ramani, *J. Electrochem. Soc.* **2014**, *161*, F1 – F9.

[14] M. H. Kuchma, C. B. Komanski, J. Colon, A. Teblum, A. E. Masunov, B. Alvarado, S. Babu, S. Seal, J. Summy, C. H. Baker, *Nanomed. Nanotechnol. Biol. Med.* **2010**, *6*, 738 – 744.

[15] a) S.-B. Hong, F. M. Raushel, *J. Enzyme Inhib.* **1997**, *12*, 191 – 203; b) C. R. Samples, F. M. Raushel, V. J. DeRose, *Biochemistry* **2007**, *46*, 3435 – 3442.

[16] G. Chen, H. Zhao, F. Rosei, D. Ma, *J. Phys. Chem. C* **2013**, *117*, 10031 – 10038.

Received: November 7, 2015
Revised: November 13, 2015
Published online: December 11, 2015

